Understanding of void formation in Cu/Sn-Sn/Cu system during transient liquid phase bonding process through diffusion modeling

Sylvie Bourdineaud-Bordère, Emilien Feuillet, Jean-Luc Diot, Renaud de Langlade, Jean-François Silvain

Understanding of void formation in Cu/Sn-Sn/Cu system during Transient Liquid Phase Bonding process through diffusion modeling.

Sylvie Bordère[a], Emilien Feuillet[b], Jean-Luc Diot[c], Renaud de Langlade[c], Jean-François Silvain[a,*]

[a] CNRS, Univ. Bordeaux, ICMCB, UPR 9048, F-33600 Pessac, France

[b] Innoptics, rue François Mitterrand, 33400 TALENCE (France)

[c] Composite Innovation, 2 allée du Doyen Brus, 33600 PESSAC (France)

*Corresponding author : Institut de Chimie de la Matière Condensée de Bordeaux, ICMCB-CNRS, 87 Avenue du Dr A. Schweitzer, F-33608 PESSAC Cedex, France.

Phone : +33 (0)5 40 00 84 37

Email address : jean-francois.silvain@icmcb.cnrs.fr

Abstract

Transient Liquid Phase (TPL) bounding of Sn foil sandwiched between two Cu foils involves, in the temperature range above the melting point of Sn (232°C) and below 350°C, the formation and the growth of two intermetallic compounds (IMCs) Cu_6Sn_5 and Cu_3Sn and mostly unintended micro-pores. The present study aims to analyze the mechanism of void development during the soldering process through an experimental and modeling approach of diffusion controlled IMC transformation. This modeling couples the diffusion process and the interface motion with the volume shrinkage induced by the difference of partial molar volumes of atoms between each phase. We also consider two types of inter-diffusion transports: i) inter-diffusion based on the exchange of Cu and Sn-atoms and ii) inter-diffusion of Sn atoms with vacancies allowing Kirkendall void formation. The simulations of IMC growth performed corresponds to a sequence of planar phase layers, where the distinctive scallop morphology of the Cu_6Sn_5 layer is described through an analytical function allowing to quantify the grain boundary diffusion pathway. We take into account of the volume diffusion mechanism for Cu_3Sn intermetallic. For Cu_6Sn_5 intermetallic two mechanisms are considered, volume diffusion and grain boundary

diffusion, limited by grain growth. The simulations of IMC growth kinetics, for different transport scenarios, are compared to the experimental evolving morphologies to determine the most likely mechanism of micro-void formation.

Keywords: Transient liquid phase bounding; Intermetallics; Cu-Sn; Diffusion; void formation and growth; Simulations.

1. Introduction

The current trend of power electronic modules towards higher power densities and higher junction temperatures requires the development of new interconnect technologies that are able to withstand cyclic thermomechanical stresses at temperatures higher than 200°C. Indeed, classical packaging technologies, such as soft soldering and wire bonding, are the limiting factors for better performance of power modules [1].

One promising interconnect technology for high temperature applications is the Transient Liquid Phase Bonding (TLPB) process [2]. This technique relies on the formation of intermetallic compounds (IMCs) as a bonding medium involving a liquid phase which is progressively consumed. The process employs a binary system consisting of two metals (or metal alloy) with different melting points: a low-melting point interlayer, such as tin (Sn), sandwiched between two high-melting point substrates, such as copper (Cu). The choice of the Cu-Sn system was motivated first by the widespread use of Cu-metal in electronic packaging, in particular as metallization layers on ceramic substrates, and secondly by the low melting point (232°C) of Sn-metal, together with its ability to form IMCs with Cu, and its low cost. Upon heating to typical bonding temperature, just above Sn melting point, the Cu substrates react with the liquid Sn trough inter-diffusion. According to the Cu-Sn phase diagram [3,4], two IMCs, Cu_6Sn_5 and Cu_3Sn, form and grow through isothermal condition. The goal of the process is to entirely transform the Sn interlayer into the Cu-rich IMC, Cu_3Sn. This phase is thermodynamically stable up to 350°C and has a re-melting temperature (676°C) much higher than the process temperature.

The growth kinetics and the evolving morphologies of the IMCs during TLP soldering are highly dependent on the process parameters: heating rate and bonding temperature, compressive stress for layer contact [5] and initial thickness of the Sn foil [6]. Nevertheless, within the bonding temperature range [240°C-280°C] the following growth sequence was observed. The Cu_6Sn_5-phase growth dominates, that of the Cu_3Sn-phase, in the early stages of the process. It is only when the Sn liquid phase is entirely consumed that the Cu_3Sn layer grows at the expense of the previously formed Cu_6Sn_5-layer. Moreover, the Cu_6Sn_5-layer does not grow in a flat but rather in a rough way associated with a rounded grains morphology called scallops [7]. High coarsening rate gives rise to some large Cu_6Sn_5 scallops on the two opposite diffusion front which quickly impinge before the complete transformation of Sn into IMCs [2]. Such early scallop impingement is expected to be the necessary condition for the formation of voids in the bond mid plane during TLP bounding [8]. The presence of such voids decreases the IMC bonds reliability as well as their thermal and mechanical properties, and should be therefore limited as much as possible. Many experimental studies have so focused on the way to inhibit the development of micro-voids. They have shown that favorable conditions are high bonding temperature, high heating rate [5], low Sn foil thickness [6] and high contact pressure [5]. Simulation works of Park and coworkers also investigated the microstructure evolution during TLP bonding process using the multi-phase field modeling together with thermodynamics and kinetics databases (CALPHAD) [9-11]. They provide, through the variation of the model parameters and experimental comparisons, a valuable insight into the kinetic growth of the IMC layers, the morphological evolution and especially the parameter conditions for high interface roughness that is one of the key points for further voids development. Nevertheless, these simulation works do not account for the mechanism of the pore formation which remains a challenge for the complete understanding of IMC bounding mechanism. Some authors have suggested, through the studies of TLP bonding of equivalent Ag/Sn/Ag [12] and Ni/Sn/Ni [13] sandwich structures that the observed void formation is due to the difference in molar volume between the initial reacting phases and IMC products leading to volume shrinkage. Similarly, the molar volume properties of the Cu_6Sn_5-phase, $Cu_{(s)}$ and $Sn_{(l)}$-reactants give rise to about 8.5% [14] of volume shrinkage. So, when the Cu_6Sn_5-scallops on the two opposite layers impinge, the reaction progress within a fixed $Sn_{(l)}$ volume allowing the pore formation. The pore volume is thus expected to be lower than 8.5% of the overall

Cu_6Sn_5 volume, the later the scallop impingement occurs the lower the volume fraction of the pores formed. Therefore, volume shrinkage seems to underestimate the large pore volume observed which can reach the high value of 25 % of the IMC layer [5]. Other type of voids, due to Kirkendall effect [15], can also form in the IMC layers. Their formation is the result of the difference between the diffusion rates of Cu and Sn which is counterbalanced by the transport of atomic vacancies [16-17]. The aggregation of vacancies generates Kirkendall voids inside the compound behind the migration of the atoms which diffuse faster. For the Cu_3Sn layer, the intrinsic diffusion coefficient of Cu-atoms is shown to be much larger than the Sn atom one, with a ratio around 7 at 150°C [16] and 30 at 200°C [18]. This difference in diffusion coefficient confirmed that Kirkendall voids are present at the Cu_3Sn/Cu interface under the Sn melting point [16-17]. For the Cu_6Sn_5-layer, some controversy about whether the Cu-atoms diffuse faster or not exists. As it is generally held, the diffusion rate of Cu-atoms was determined to be greater than that of Sn atoms in some studies [19-20] whereas it was found lower in other [18]. In the case where Sn-atoms diffuse faster than Cu-atoms in the Cu_6Sn_5 layer, Kirkendall voids may also form in the Cu_6Sn_5 interlayer, but the question remains whether such mechanism would account for such micro-void formation.

The complete understanding of the mechanism of the pore formation during IMC bounding still remains a challenge. In this paper, our main objective is to get an insight of pore formation through a modeling approach of diffusion controlled phase growth involving different mass transport mechanisms and volume shrinkage inherent to the difference of the Cu and Sn partial molar volumes between each involving phases.

In a first step, we will reinvestigate bonding tests for experimental parameters favoring the development of macro-voids to easily compare the remaining $Sn_{(l)}$ volume at the Cu_6Sn_5 scallop impingement with that of micro-voids. In a second step, 1D-simulations of the evolution of phase volume fractions and pore volume fraction will be performed by considering, i) inter-diffusion of Sn atoms with Cu atoms or vacancies, ii) partial molar volume induced shrinkage, iii) volume diffusion or grain boundary diffusion as limiting transport processes. The comparison between experimental and numerical results, will allow us to determine the most likely mechanisms for IMC growth and macro-void formation during TLB process.

2- Experimental part

2.1 Formation of IMC joint

The formation of a joint entirely composed of intermetallic compounds (IMC), which shows a higher thermal cycling reliability than the reference SnAgCu solder alloys, using the Transient Liquid Phase Bonding process (TLPB) based on the copper-tin binary system, has already been described by several authors [2, 8, 21-24]. Figure 1 shows the binary Cu-Sn phase diagram (Fig. 1f) and the different steps linked with this IMC joint formation (Fig. 1a to 1e). In the first step, the system is heated at 250°C, just above the melting temperature of Sn (232°C), leading to a complete wetting of the Cu substrate by the liquid Sn (Fig. 1a) and spontaneous dissolution of the Cu substrate inside the liquid Sn leading to a supersaturated Sn liquid phase. In the second step, dissolution of part the Cu substrate continue and nucleation of the first Cu_6Sn_5 intermetallic germs (η phase) begun (Fig. 1b). Then, the isotherm solidification of the IMC joint, at 250°C, start associated with the growth of Cu_6Sn_5 intermetallic with 3D column like shape, also called scallops, (Fig. 1 c) and the growth of 2D Cu_3Sn one (ε phase) [25]. The chemical reaction (6 Cu + 5 Sn -> Cu_6Sn_5) end when all the liquid Sn is transformed to solid Cu_6Sn_5 (Fig. 1 d). Finally, transformation of Cu_6Sn_5 to Cu_3Sn continues up to a complete consumption of Cu_6Sn_5 intermetallic (Fig. 1e).

(Fig. 1e).

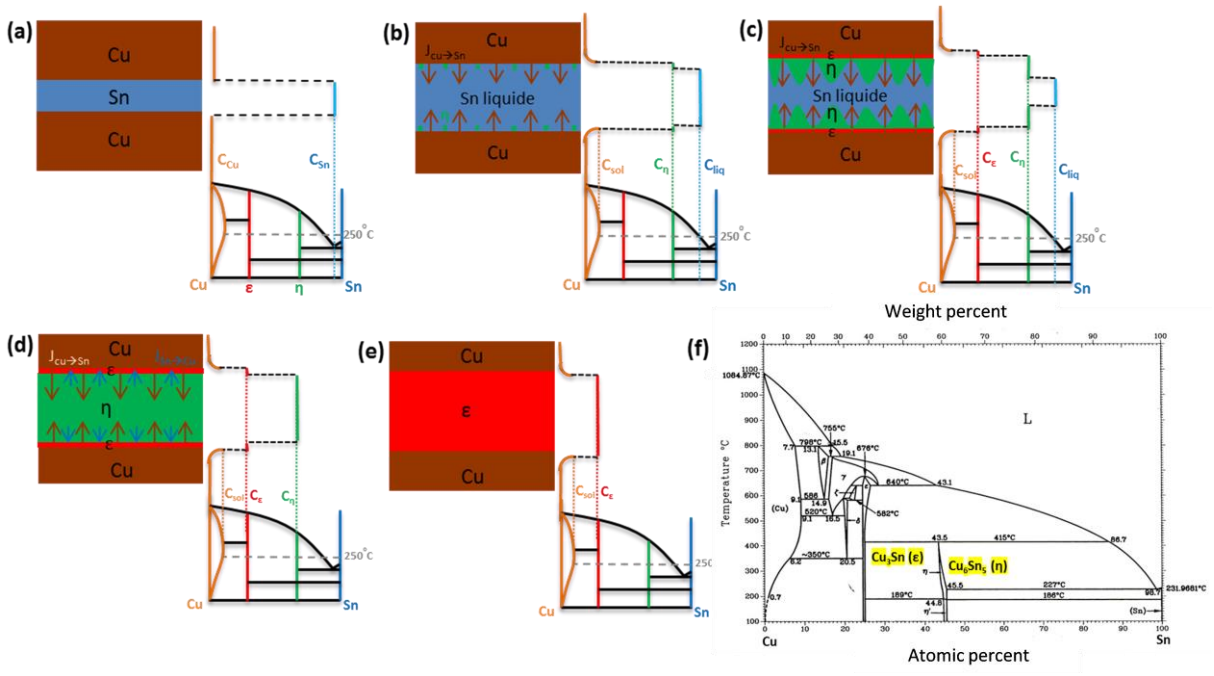

Figure 1: Different steps of the IMC report using TLPB based on Cu-Sn system. a) Fusion of the Sn filler metal (liquid Sn in blue color), b) Dissolution of part of the Cu substrate inside liquid Sn and nucleation of first Cu_6Sn_5 germs, c) Growth of both Cu_6Sn_5 and Cu_3Sn IMCs and consumption of remaining liquid Sn d) Complete consumption of liquid Sn and solidification of the IMC joint, e) Homogenization of the joint toward the most stable Cu_3Sn intermetallic, f) Cu-Sn binary phase diagram (Reprinted from reference [3]).

2.2 Evolution of the IMC morphology, chemical composition and volume fraction with holding time

However, in that theoretical process, porosity is not considered which is not exactly the case for a real IMC joint. A specific experimental apparatus has been used for the formation of the IMC joints. It is composed of a hermetic metallic chamber with 2 heating plates separately controlled with 2 temperature regulators. Temperature is measured with 2 k thermocouples. The pressure is applied with the lower plate using a hydraulic system. The chamber is working under secondary vacuum (10^{-3} mbar). After surface cleaning using hydrochloric acid (5%), Copper substrates are coated with Sn thin film using conventional PVD system.

Figure 2 shows the evolution of a real IMC joint for a fixed temperature and pressure and for different holding time. For a holding time of 0 min and for a process temperature (250°C) above the melting temperature of Sn (232°C), the dissolution of Cu inside Sn (red arrows) is associated with a 3-dimensional (3D) growth of Cu-Sn intermetallic (mainly Cu_6Sn_5 one) at the Cu-Sn interface (Fig. 2a). At the same holding stage (0 min) the composition of the Cu-Sn reaction zone has been analyzed using line profile Auger electron spectroscopy (Fig. 2b). The line profile clearly shows the Cu substrate, the Cu-Sn reaction zone composed of the 2 intermetallics Cu_3Sn and Cu_6Sn_5. For a holding time of 5 min, the growth of 3D Cu_6Sn_5 intermetallic and 2D Cu_3Sn one is clearly shown (Fig. 2c). Continuous precipitation of Cu_6Sn_5 at the surface of the 3D Cu_6Sn_5 hemispheric intermetallics (green arrows in Fig. 2c) induces the vertical growth of the intermetallics (blue arrow in Fig. 2c) up to a contact green dashed line Fig. 2d) and chemical link between 2 facing hemispherical Cu_6Sn_5 scallops (labeled (1) and (2) in Fig. 2d) growing from both Cu substrate. At that stage, the thickness of the IMC joint become fixed and lateral growth (for example blue arrows in Fig. 2d) of the intermetallic take place up to a complete consumption of the liquid Sn (Fig. 2f). Up to a complete consumption of liquid Sn, the growth kinetic of the Cu_3Sn intermetallic is very slow and, for our system, it thickness is smaller than 1 μm. When the the liquid Sn is completely consumed (Fig. 2f), one can observe two sorts of pores in the Cu_6Sn_5 IMC; small ones located near the Cu_3Sn IMC, and large ones which can fill nearly all the gap between the 2 Cu_3Sn IMC layers. We can suppose that the pores are initially formed in the liquid channel near the Cu_6Sn_5-Sn interface, as observed in Fig 2e (blue arrow). Some of the pores are then trapped within the Cu_6Sn_5 IMC during IMC growth (green arrows in Fig. 2e) and the others can growth toward the liquid phases (white arrows) to formed large porosities.

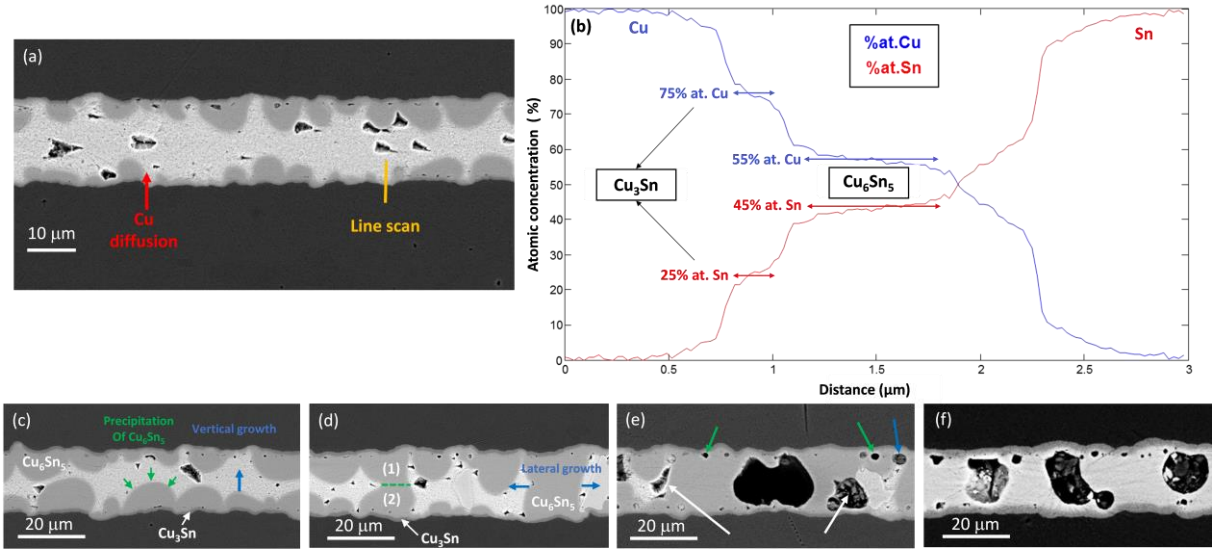

Figure 2: Experimental formation of Cu-Sn IMC joint for different holding time for a 5 KPa pressure and a holding temperature of 250°C. a) SEM micrograph at 0 min, b) AES line profile at 0 min, c) SEM micrograph at 15 min, d) SEM micrograph at 30 min, e) SEM micrograph at 45 min, f) SEM micrograph at after complete reaction of liquid Sn (2 hours)

Color scale (a-e) (darker to lighter gray): Cu substrate; Cu_3Sn; Cu_6Sn_5, Sn

Color scale (f) (darker to lighter gray): Cu substrate; Cu_3Sn; Cu_6Sn_5

2.3 Evolution of the IMC morphology and chemical composition with holding temperature

Figure 3 shows the evolution of IMC Cu-Sn joints for pressure and holding time of report of 5 KPa and 120 min respectively and for 3 holding temperature (250°C, 270°C and 300°C). On that figure, for a same initial Sn thickness (thin fil close to 20 µm), the thickness of the IMC joints decreases when the holding temperature increases. This behavior is linked with the decrease of the viscosity of the liquid Sn with the temperature and the ejection of part of the liquid Sn due to the 5 KPa pressure used. It can be observed that large pores are present in the middle of the joint whatever the holding temperature even when all the Cu_6Sn_5 phase has been transformed into Cu_3Sn (Fig. 3c). Therefore, the volume fraction of porosity can vary from 10 to 20% depending on the elaboration condition and on the volume fraction of the IMCS in the joint.

Finally, the increase of diffusion fluxes with the temperature induces an increase of the Cu_3Sn intermetallic growth. At 300°C, all the Cu_6Sn_5 intermetallic is transformed to Cu_3Sn one after just 2 hours (Fig. 3c). The two sorts of voids, previously observed in the Cu_6Sn_5 IMC (Fig. 2e), still remain for this equilibrium microstructure: large pores in the middle of the Cu_3Sn joint and smaller ones closer to the Cu_3Sn/Cu interface. Such groups of pores were already observed for this end state [26].

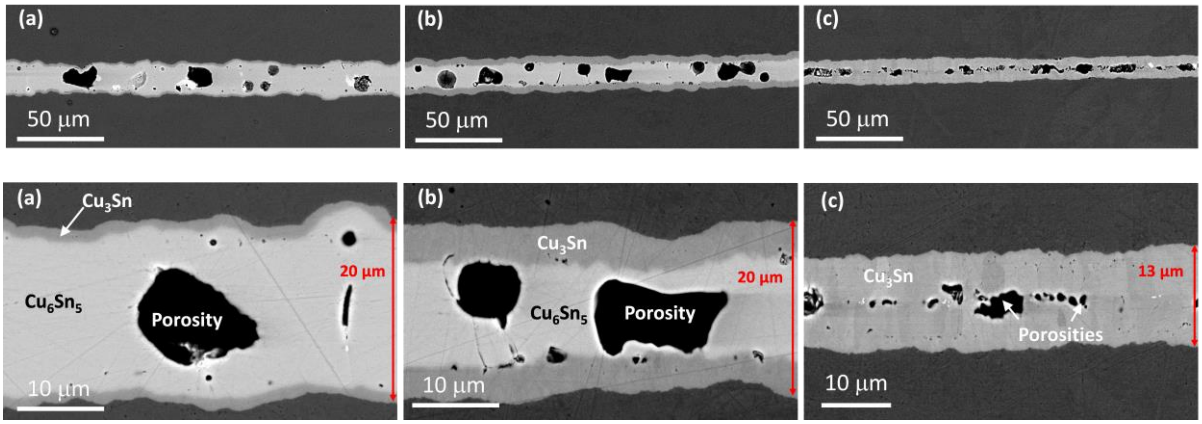

Figure 3: Evolution of the IMC morphology and chemical composition with holding temperature (pressure of 5 KPa and holding time of 120 min): a) 250°C, b) 270°C and c) 300°C

Color scale (a-c) (darker to lighter gray): Cu substrate; Cu_3Sn; Cu_6Sn_5

3 – Modelling of the formation of the Cu/Sn-based solder joint

3.1 Description of the physical equations

The formation of the Cu_6Sn_5 and Cu_3Sn IMCs in the Cu-Sn solder are considered to evolve through diffusion controlled phase changes. This is described by equations based on inter-diffusion of Sn and Cu-atoms. It means that to any Cu-flux, a strictly opposite Sn-flux is involved. In this diffusion modeling, we chose to only describe the Sn flux. The governing equation of the Sn flux $\mathbf{J}_{Sn}^{i}(X,t)$ within each involved phase *i* (*i*=1,…4), at each time *t* and position **X** of the system, is based on the first Fick's diffusion law written as:

$$\mathbf{J}_{Sn}^{i}(\mathbf{X},t) = -D^{i}(\mathbf{X},t)\,\nabla C_{Sn}^{i}(\mathbf{X},t)\,. \qquad (1)$$

Here, $D^{i}(\mathbf{X},t)$ and $C_{Sn}^{i}(\mathbf{X},t)$ are respectively the inter-diffusion coefficient of the Cu/Sn-couple and the Sn-molar concentrations relative to the *i*-phase, at the position **X** and the evolution time *t*.

For non-stationary diffusion regime, mass conservation requires the use of the second Fick's law written as:

$$\nabla \cdot \mathbf{J}_{Sn}^{i}(\mathbf{X},t) = -\frac{\partial}{\partial t} C_{sn}^{i}(\mathbf{X},t) \tag{2}$$

Moreover, when the flux balance at the interface I_i between two adjacent i and i+1 phases is non-zero, the Sn-molar concentrations $C_{Sn}^{i}(\mathbf{X}_{I_i},t)$ and $C_{Sn}^{i+1}(\mathbf{X}_{I_i},t)$ at the I_i-interface are kept consistent with thermodynamics by interface displacement. The normal displacement rate of a point of the interface positioned at $\mathbf{X}_{I_i}(t)$ is defined at time t as:

$$\frac{dX_{I_i}(t)}{dt} = \frac{\left(\mathbf{J}_{Sn}^{i}(\mathbf{X}_{I_i},t) - \mathbf{J}_{Sn}^{i+1}(\mathbf{X}_{I_i},t)\right)\cdot\mathbf{n}}{\left(C_{Sn}^{i}(\mathbf{X}_{I_i},t) - C_{Sn}^{i+1}(\mathbf{X}_{I_i},t)\right)} \tag{3}$$

The difference between the Cu and Sn-partial molar volumes, of the phase i-phase ($\overline{V}_{cu}^{i}$ and $\overline{V}_{Sn}^{i}$) and that of the i+1-phase ($\overline{V}_{cu}^{i+1}$ and $\overline{V}_{Sn}^{i+1}$), induces additional normal displacement of the I_i-interface to relax the elastic strain within the phase transition area. This displacement, $dX_{I_i}^{R_1}$, is written through two equivalent equations involving either the i-phase (Eq. (4a)) or the i+1-phase (Eq. (4b)).

$$\begin{aligned}\frac{dX_{I_i}^{R_1}(t)}{dt} = &\left(\mathbf{J}_{Sn}^{i}(\mathbf{X}_{I_i},t) - C_{Sn}^{i}(\mathbf{X}_{I_i},t)\frac{dX_{I_i}(t)}{dt}\right)\left(\overline{V}_{Sn}^{i+1} - \overline{V}_{Sn}^{i}\right) \\ &+\left(\mathbf{J}_{Cu}^{i}(\mathbf{X}_{I_i},t) - C_{Cu}^{i}(\mathbf{X}_{I_i},t)\frac{dX_{I_i}(t)}{dt}\right)\left(\overline{V}_{Cu}^{i+1} - \overline{V}_{Cu}^{i}\right)\end{aligned} \tag{4a}$$

$$\begin{aligned}\frac{dX_{I_i}^{R_1}(t)}{dt} = &\left(\mathbf{J}_{Sn}^{i+1}(\mathbf{X}_{I_i},t) - C_{Sn}^{i+1}(\mathbf{X}_{I_i},t)\frac{dX_{I_i}(t)}{dt}\right)\left(\overline{V}_{Sn}^{i+1} - \overline{V}_{Sn}^{i}\right) \\ &+\left(\mathbf{J}_{Cu}^{i+1}(\mathbf{X}_{I_i},t) - C_{Cu}^{i+1}(\mathbf{X}_{I_i},t)\frac{dX_{I_i}(t)}{dt}\right)\left(\overline{V}_{Cu}^{i+1} - \overline{V}_{Cu}^{i}\right)\end{aligned} \tag{4b}$$

If this displacement allows relaxing locally the elastic strain within the phase transformation area, it nevertheless induces elastic strain within the neighboring phases, depending on their elastic properties and on the boundary conditions of the mechanical problem. This second step of elastic strain energy

relaxation potentially involves the normal displacement $dX_{I_i}^{R_2}$ of the entire interface I_i of the system. The complete modeling equations of this second step of elastic strain relaxation is complex and is not described in this paper.

Note that the displacements $dX_{I_i}^{R_1}(t)$ and $dX_{I_i}^{R_2}(t)$ of the I_i-interfaces during time interval *dt*, implies an advection along the displacement field of the molar concentrations $C_{Sn}^{i}(\mathbf{X},t+dt)$ previously determined from the diffusion equation solving.

3.2 Numerical procedure for the one-dimensional problem

3.2.1 Description of the one-dimensional system

The complex growing morphology of the Cu_6Sn_5 and Cu_3Sn layers in the Sn based solder-Cu system is reduced to a one-dimensional problem of a succession of planar layers of surface S (Fig. 4). Such planar geometry has been considered for analytical models of intermetallic layer growth, which nevertheless need numerical approaches to be solved [14, 27]. Here, the possible development of a vapor phase as well as the description of the morphology evolution through an analytical function (see paragraph 3.2.2.) make that diffusion equations are solved numerically using time-step procedure. Each layer is indexed in agreement with the experimental phase sequence. Note that the vapor phase in not indexed. The constant dimension of the system implies that the scalar position X_{I_0} and X_{I_L} are fixed. The X_{I_0}-position is a cut-off point within the large width of the $Cu_{(s)}$-phase and the X_{I_L} - position is a symmetry point allowing to represent the two layers of the overall experimental system (Fig. 4). The thickness of each layer at time *t* can thus be determined from the position on the *X*-axis of the interfaces $Cu_{(s)}$-Cu_3Sn (I_1), Cu_3Sn-Cu_6Sn_5 (I_2), Cu_6Sn_5-$Sn_{(l)}$ (I_3) and $Sn_{(l)}$-$Sn_{(v)}$ (I_4) noted as $X_{I_1}(t)$, $X_{I_2}(t)$, $X_{I_3}(t)$ and $X_{I_4}(t)$, respectively (Fig. 4).

The Sn molar concentrations $C_{Sn}^{i}(I_i)$ and $C_{Sn}^{i+1}(I_i)$ at the I_i-interface (i=1,3) (Fig. 4) correspond to the local equilibrium values and are thus constant during phase transformations. They are determined from the Sn molar fractions $x_{Sn}^{i}(I_i)$ and $x_{Sn}^{i+1}(I_i)$ relative to the Cu-Sn phase diagram [3] for the temperature

of 250 °C, and from the partial molar volumes of Cu ($\overline{V}_{cu}^{i}$) and Sn ($\overline{V}_{sn}^{i}$) relative to the *i*-phase. They can be expressed through the following equation.

$$C_{Sn}^{i}(I_j)=\frac{x_{sn}^{i}(I_j)}{x_{sn}^{i}(I_j)\overline{V}_{sn}^{i}+\left(1-x_{sn}^{i}(I_j)\right)\overline{V}_{Cu}^{i}};\ i=j,\ j+1;\ j=1,3 \qquad (5)$$

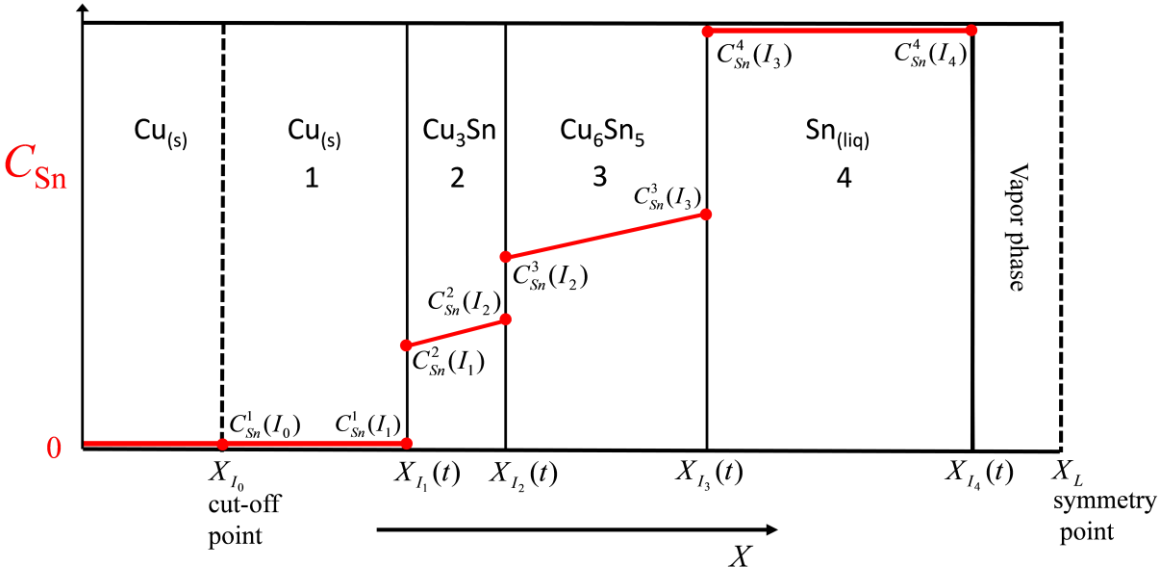

Figure 4: One-dimensional problem of the Cu_6Sn_5 and Cu_3Sn layers in the Sn based solder-Cu system using linear profile of Sn molar concentrations $C_{Sn}^{i}(X,t)$ within each phase *i*.

The values of the Sn-molar fractions $x_{Sn}^{i}(I_j)$ (j=i-1; i=2, 4; $j\leq 3$) are indicated in table 1 and the partial molar volumes $\overline{V}_{cu}^{i}$ and $\overline{V}_{sn}^{i}$ (i = 1, 4) in table 2. For solving the diffusion problem, we have made the following assumptions illustrated in figure 4:

i) $Cu_{(s)}$ phase (i=1) is considered Sn saturated $C_{Sn}^{1}(I_1)=C_{Sn}^{1}(I_0)$ near the I_1-interface i.e. within the width $[X_{I_0}, X_{I_1}(t)]$. This assumption has low impact on the evolution of the phase volume fractions since the two conditions, $J_{Sn}^{1}(X,t)=0$ and $x_{Sn}^{1}(I_1)=0.022\approx 0$ are compatible with a very low diffusion coefficient which is more than nine order of magnitude lower than the diffusion coefficient of the others involved phases (see Table 2).

ii) Sn-molar concentration $C_{Sn}^{i}(X,t)$ within the IMCs Cu_3Sn (i=2) and Cu_6Sn_5 (i=3) are linear from the molar concentration $C_{Sn}^{i}(I_{i-1})$ to $C_{Sn}^{i}(I_i)$ at the interfaces I_i-1 and I_i, respectively.

iii) $Sn_{(l)}$-phase is considered Cu-saturated $C_{Sn}^{4}(I_4) = C_{Sn}^{4}(I_3)$ (Fig. 4).

iv) Inter-diffusion coefficient $D^i(X,t)$ characterizing the i-phase is assumed independent of the Sn molar concentration. The constant values of inter-diffusion coefficients D^i are indicated in table 2.

Interface	$Cu_{(s)}$-Cu_3Sn		Cu_3Sn-Cu_6Sn_5		Cu_6Sn_5-$Sn_{(l)}$	
Sn molar fraction	$x_{Sn}^{1}(I_1)$	$x_{Sn}^{2}(I_1)$	$x_{Sn}^{2}(I_2)$	$x_{Sn}^{3}(I_2)$	$x_{Sn}^{3}(I_3)$	$x_{Sn}^{4}(I_3)$
	2.2	23.6	24.7	44.5	45.4	97.8

Table 1: Sn-molar fractions at the different interfaces involved in the Cu-Sn system with reference to the phase diagram for a temperature of 250 °C [3].

Phase i	$Cu_{(s)}$ (i = 1)	Cu_3Sn (i = 2)	Cu_6Sn_5 (i = 3)	$Sn_{(l)}$ (i = 4)
Sn partial molar volume $\overline{V}_{Sn}^{i}$ (cm^3/mol)	16.3[b]	15.9[a]	15.9[a]	17.0[b]
Cu partial molar volume $\overline{V}_{Cu}^{i}$ (cm^3/mol)	7.1[c]	6.2[a]	6.2[a]	7,3[c]
Inter-diffusion coefficient D^i (m^2/s)	$1.0x10^{-22}$[e]	$3.6x10^{-15}$[d]	$7.6x10^{-15}$[d]	$2.0x10^{-9}$[f]

Table 2: Partial molar volumes of Sn and Cu-atoms and inter-diffusion coefficients for the phases involved in the Sn-based solder/Cu system: [a]deduced from the lattice parameter data available in the literature [28]; [b]deduced from the density of liquid tin at 250°C [29] and from the 3% variation for the liquid/solid transition as determined in [30] for the $Cu_{(s)}$-phase; [c]deduced from the density of copper at 250°C and from the extrapolation at 250°C of the linear variation of liquid copper density for the $Sn_{(l)}$-phase [31]; [d]calculated at 250°C from Arrhenius equation defined in [14]. They are close to that we can obtain from other references [32-33]; [e]calculated at 250°C from Arrhenius equation defined for 2% of Sn in [34]; [f]close to $Sn_{(l)}$ self-diffusion coefficient [35].

3.2.2 Morphology function for Cu_6Sn_5-layer

The distinctive scalloped morphology of the Cu_6Sn_5-layer is described by the hexagonal-base/spherical-cap geometric model of Schaefer et al. [25] (Fig. 5a). In this model, each scallop corresponds to a grain and each grain is characterized by uniform evolving morphology and grain size. The molten channel connected to grain boundaries is here represented leading to a shortened average diffusion distance along these grain boundaries (d_{GB}) in comparison with the volume diffusion distance similar to the average thickness (d_L) (Fig. 5b). The effective area available for grain boundary diffusion represents a small fraction (f) of the layer surface. Assuming hexagonal grains with diagonal size, d, and constant width distance δ, this fraction was defined as [25]:

$$f = \frac{\delta}{\sqrt{3}d} \tag{6}$$

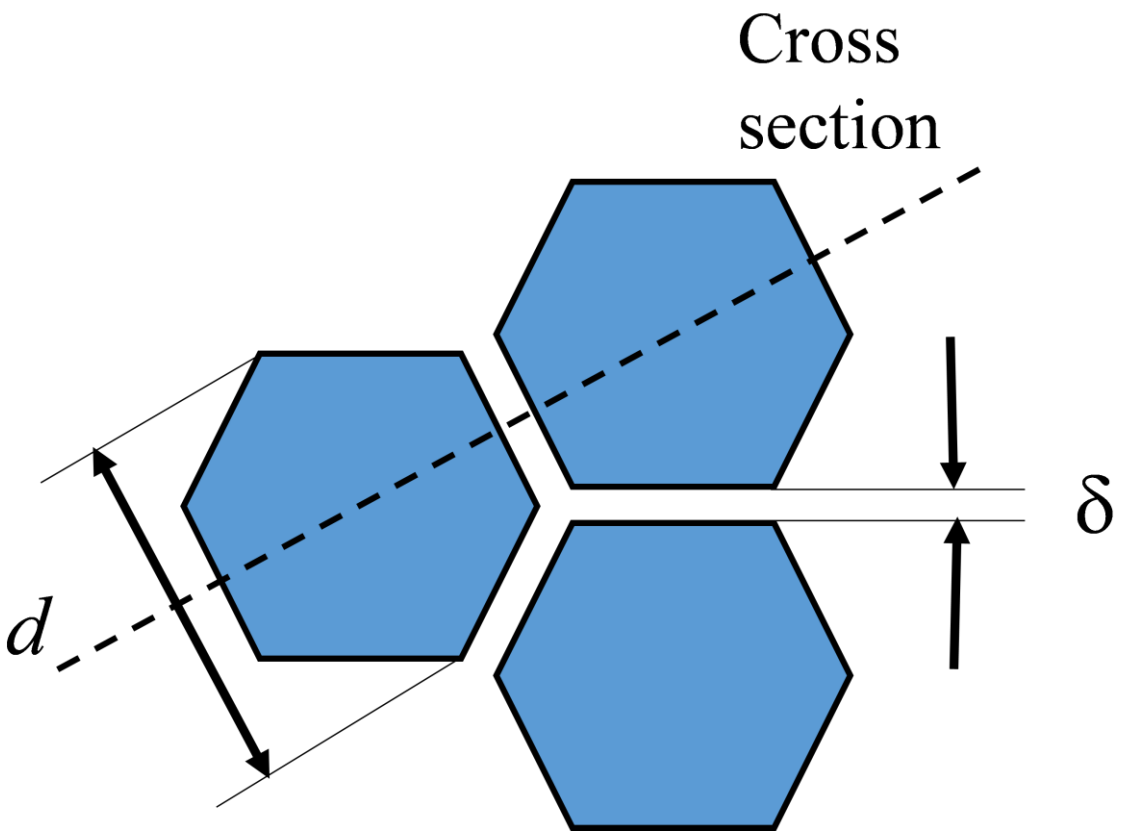

a)

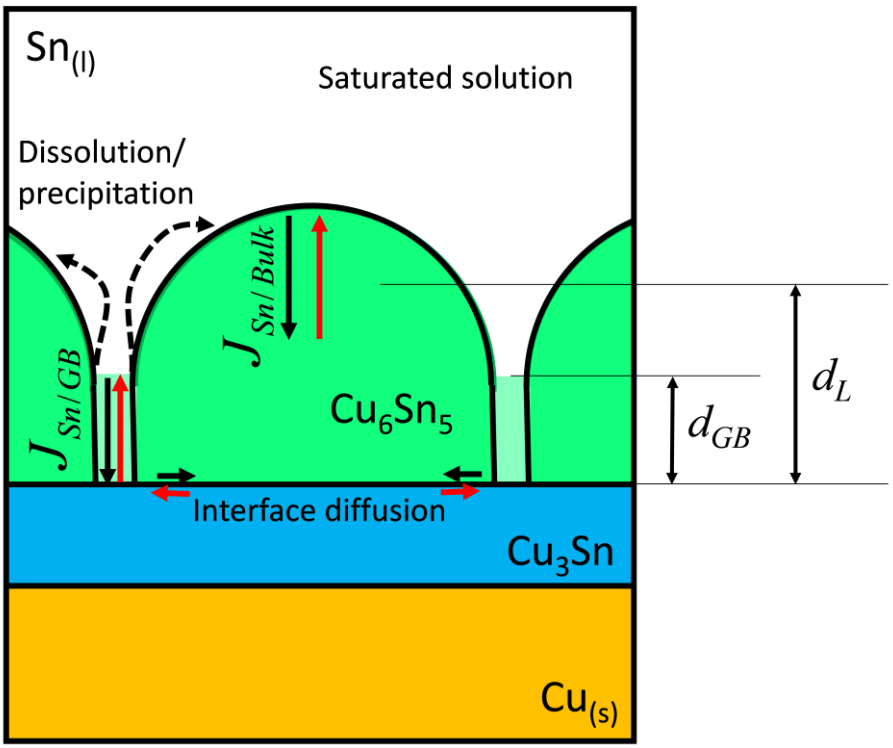

b)

Figure 5: Geometric model for the microstructure of the Cu_6Sn_5-layer described in [25]. (a), top view of the layer showing grain size d and grain boundary width δ. (b), cross section corresponding to the dashed line in (a) showing the average layer thickness d_L and the average grain boundary length d_{GB}.

→ Sn-fluxes in the bulk and along grain boundaries of the Cu_6Sn_5-layer and along the Cu_3Sn/Cu_6Sn_5 interface

→ Reverse Cu-fluxes of equal intensity in the case of inter-diffusion

3.2.3 Solving procedure for volume and grain boundary inter-diffusion and volume shrinkage

In the following, only the Sn fluxes are solved since inter-diffusion mass transport means that to any Sn fluxes is associated reverse Cu fluxes of equal intensity. So, when it is not specified, the term "flux" is always related to Sn flux. The one-dimensional system approximation reduces the fluxes to be perpendicular to the layer. The total flux $J^i_{Sn}(X,t)$ through each phase (i = 1, 4) corresponds to the contribution of volume flux $J^i_{Sn/Vol}(X,t)$ and grain boundary flux $J^4_{Sn/GB}(X,t)$ through the relation below.

$$J^{i}_{Sn}(X,t) = J^{i}_{Sn/Vol}(X,t) + J^{i}_{Sn/GB}(X,t) \quad (7)$$

The total fluxes at the interfaces I_{i-1} and I_i relative to the *i*-phase written as $J^{i}_{Sn}(X_{I_{i-1}},t)$ and $J^{i}_{Sn}(X_{I_i},t)$ respectively, are determined using the following assumptions.

- No fluxes are involved through the $Cu_{(s)}$-phase (negligible diffusion) and $Sn_{(l)}$-phase (saturated solution):

$J^{1}_{Sn}(X_{I_0},t) = J^{1}_{Sn}(X_{I_1},t) = 0$ and $J^{4}_{Sn}(X_{I_3},t) = J^{4}_{Sn}(X_{I_4},t) = 0$

- Volume diffusion is the predominant mechanism within the Cu_3Sn-phase [2, 5, 20, 26]; molar concentration profile (Fig. 4) at time *t* gives using Eq. (1),

$$J^{2}_{Sn}(X_{I_1},t) = J^{2}_{Sn}(X_{I_2},t) = J^{2}_{Sn/vol}(X,t) = -D^{2}\frac{C^{2}_{Sn}(I_2) - C^{2}_{Sn}(I_1)}{\left(X_{I_2}(t) - X_{I_1}(t)\right)}.$$

- Grain boundary diffusion is considered to be competitive with volume diffusion within the Cu_6Sn_5-scalloped phase [2, 18]. Grain boundary flux is characterized by:

$J^{3}_{Sn/GB}(X,t) = -f\ D^{3}_{GB}\dfrac{C^{3}_{Sn}(I_3) - C^{3}_{Sn}(I_2)}{d_{GB}}$, where D^{3}_{GB} is the grain boundary inter-diffusion coefficient.

Moreover, assuming that:

i) Scallop shape remains constant during layer growth we have, $d_{GB} = R \times d_L = R \times \left(X_{I_3}(t) - X_{I_2}(t)\right)$, with *R* constant;

ii) Scallops are equiaxed during layer growth, we have $d = X_{I_3}(t) - X_{I_2}(t)$ which corresponds to a grain coarsening process;

iii) Grain boundary diffusion constant D^{3}_{GB} is proportional to the volume diffusion constant through the relation, $D^{3}_{GB} = R_D \times D^{3}$;

We finally have:

$$J_{Sn}^{3}(X_{I_3},t)=J_{Sn}^{3}(X_{I_2},t)=J_{Sn}^{3}(X,t)$$

$$=-D^{3}\left((1-f)+\frac{\delta\,R_D}{\sqrt{3}\,R\left(X_{I_3}(t)-X_{I_2}(t)\right)}\right)\frac{C_{Sn}^{3}(I_3)-C_{Sn}^{3}(I_2)}{X_{I_2}(t)-X_{I_3}(t)} \quad (8)$$

Then, the flux balance at the interfaces I_i (i=1, 3) allows calculating the I_i-interface displacement $\Delta X_{I_i}(t)$ during the time increment Δt using Eq. (3) and the interface fluxes just defined:

$$\Delta X_{I_i}(t)=\frac{\left(J_{Sn}^{i}(X_{I_i},t)-J_{Sn}^{i+1}(X_{I_i},t)\right)\Delta t}{C_{Sn}^{i}(I_i)-C_{Sn}^{i+1}(I_i)}\,. \quad (9)$$

The flux values $J_{Sn}^{1}(X_{I_0},t)=J_{Sn}^{4}(X_{I_4},t)=0$, together with the boundary conditions we considered,

$$\left.\frac{\partial C_{sn}^{i}(X,t)}{\partial X}\right)_{X_{I_j}}=0,\ \text{for}\ j=0\ \text{and}\ j=4. \quad (10)$$

induce that the molar concentrations, at the two boundaries, remain constant with time, $C_{Sn}^{1}(I_0,t+\Delta t)=C_{Sn}^{1}(I_0,t)=C_{Sn}^{1}(I_0)$ and $C_{Sn}^{4}(I_4,t+\Delta t)=C_{Sn}^{4}(I_4,t)=C_{Sn}^{4}(I_4)$.

Since the molar concentration profiles (Fig. 4) induce stationary diffusion regimes $\left(\nabla\mathbf{J}_{Sn}^{i}(X,t)=0\right)$, no $C_{Sn}^{i}(X,t)$-variation is thus induced during time increment Δt (Eq. (2)) within the i-phase width $]X_{I_{i-1}}(t),X_{I_i}(t)[$. The concentration profiles at time $t+\Delta t$ are thus simply updated assuming linear X-dependence of the $C_{Sn}^{i}(X,t+\Delta t)$-molar concentration within the width $[X_{I_{i-1}}(t+\Delta t),X_{I_i}(t+\Delta t)]$ from $C_{Sn}^{i}(I_{i-1})$ to $C_{Sn}^{i}(I_i)$ values.

In a last step, we evaluate the elastic strain relaxation induced by the difference of Sn and Cu partial molar volumes from one phase to the other. The values of the Sn and Cu partial molar volumes (Table 2) show that elastic strains are not involved during transformation at the Cu_3Sn-Cu_6Sn_5 interface since the partial molar volumes are similar within the Cu_3Sn and Cu_6Sn_5 phases. Just the opposite is the difference in partial molar volumes of the $Cu_{(s)}$ and Cu_3Sn phases on one part and that of Cu_6Sn_5 and $Sn_{(l)}$ phases on the other part, which will induce tensile elastic strains during phase transformation at the $Cu_{(s)}$-Cu_3Sn and Cu_6Sn_5-$Sn_{(l)}$ interface respectively.

The displacement $\Delta X_{I_3}^{R_1}(t)$, at time *t* of the I_3-interface, induced by elastic relaxation of the transformed zone $\Delta X_{I_3}(t)$ gives, using Eq. (4b) with $J_{Sn}^4(X_{I_3},t)=J_{Cu}^4(X_{I_3},t)=0$:

$$\Delta X_{I_3}^{R_1}(t)=-\left(C_{Sn}^4(I_3)\frac{\Delta X_{I_3}(t)}{\Delta t}\right)\left(\overline{V}_{Sn}^4-\overline{V}_{Sn}^3\right)\Delta t-\left(C_{Cu}^4(I_3)\frac{\Delta X_{I_3}(t)}{\Delta t}\right)\left(\overline{V}_{Cu}^4-\overline{V}_{Cu}^4\right)\Delta t. \quad (11)$$

The displacement $\Delta X_{I_3}^{R_1}(t)$ of the I_3 interface Cu_6Sn_5-$Sn_{(l)}$ necessarily induces tensile elastic strain within the $Sn_{(liq)}$ phase. Closed boundary condition, at the I_L-interface of symmetry, together with fixed X_{I_L}-position of this interface, makes that the liquid phase can relax through the formation of a vapor phase involving the displacement $\Delta X_{I_4}^{R_2}(t)$ of the I_4-interface. Complete liquid phase relaxation leads to $\Delta X_{I_4}^{R_2}(t)=\Delta X_{I_3}^{R_1}(t)$.

Similarly, the displacement $\Delta X_{I_1}^{R_1}(t)$ of the I_1-interface induces tensile elastic strain within the $Cu_{(s)}$-phase that we can expect to be negligible in consistency with the large dimension of the experimental $Cu_{(s)}$-phase. Open boundary condition at the cut-off I_0-interface makes that an input of $Cu_{(s)}$-phase amount at constant $C_{Sn}^1(I_0)$-concentration equivalent to the length $\Delta X_{I_0}^{R_2}(t)=\Delta X_{I_1}^{R_2}(t)$ allows to obtain a zero-strain condition within this $Cu_{(s)}$ phase.

Finally, when elastic strain relaxation is considered, the position $X_{I_i}(t+\Delta t)$ of the I_i-interface (i=1,4) at time $t+\Delta t$ can be calculated from the position of the interface at time *t* through the equation:

$$X_{I_i}(t+\Delta t)=X_{I_i}(t)+\Delta X_{I_i}(t)+\Delta X_{I_i}^{R_1}(t)+\Delta X_{I_i}^{R_2}(t). \quad (12)$$

3.2.4- Solving procedure for Sn/vacancies inter-diffusion within the Cu_6Sn_5-phase

The diffusion process involving interface movement is described by equations based on inter-diffusion of Sn and Cu atoms. Here, we describe another mechanism where the Sn atoms diffuse through reverse flux of vacancies within the Cu_6Sn_5-phase only (Fig. 6). The three entities, Sn and Cu atoms and vacancies are thus considered in this mechanism. The solving methodology is done in four steps:

- As a first step, the Sn-fluxes, at the interfaces I_3 and I_2, relative to the Cu_6Sn_5 phase, are defined assuming competitive grain boundary and volume inter-diffusion Sn atoms and vacancies. Equation (8) is also here considered but using the volume inter-diffusion coefficient of Sn/vacancy couple $D^3_{Sn/L}$.

The decrease of the Sn concentration at the I_3-interface is associated to an increase of vacancy concentration. This mechanism is supposed to be counterbalanced, for interface equilibrium, by a supply of Sn atoms from the $Sn_{(l)}$ phase (Figure 6). It gives:

$$J^4_{Sn/L}(X_{I_3},t) = J^3_{Sn/L}(X_{I_3},t). \quad (13)$$

Similarly, the increase of the Sn concentration, at the I_2-interface, is counterbalanced by depletion of Sn atoms passing within the Cu_3Sn-phase (Figure 6). It gives:

$$J^2_{Sn/L}(X_{I_2},t) = J^3_{Sn/L}(X_{I_2},t). \quad (14)$$

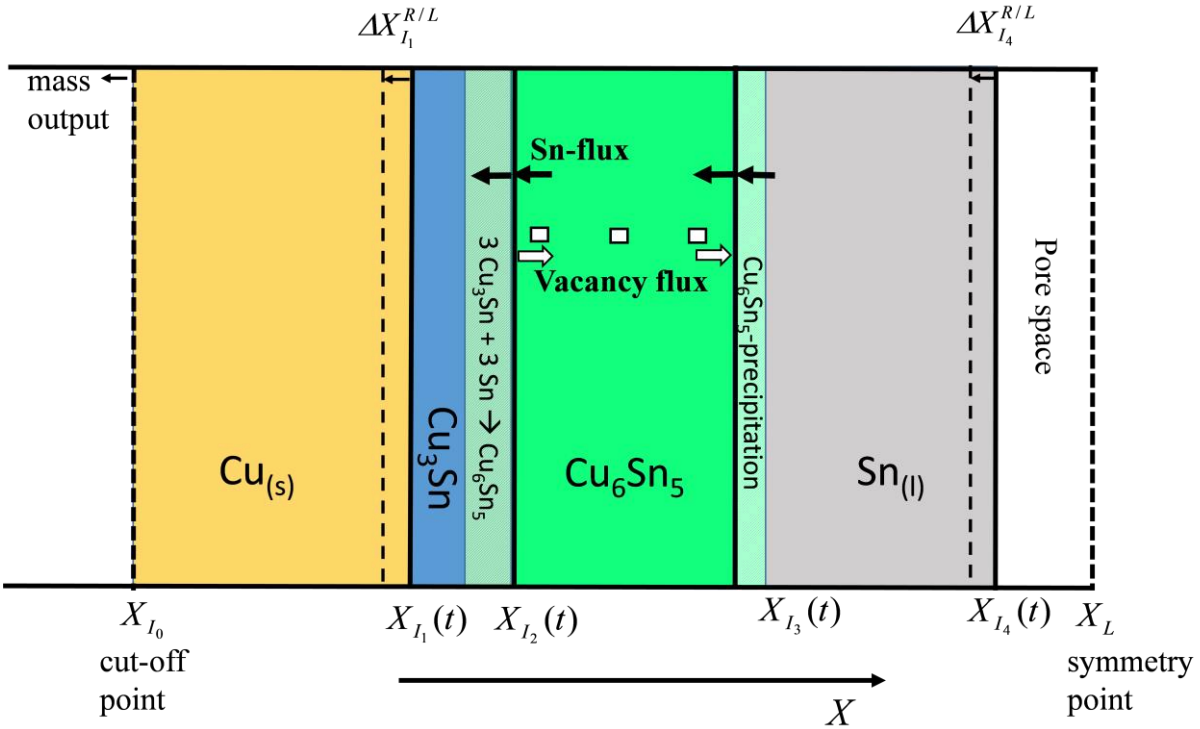

Figure 6: Schematic illustration of the mechanism of Sn/vacancy inter-diffusion within the Cu_6Sn_5-phase involving Cu_6Sn_5-growth at the interfaces I_3 and I_2 together with displacements of the I_1 and I_4 interfaces. The I_4 interface displacement induces pore formation.

This transport mechanism makes that the concentrations of Sn atoms and vacancies remain constant within the Cu_6Sn_5 phase. Equations (13) and (14) induce, with reference to Eq. (3), no displacement of the interfaces I_2 and I_3, respectively assuming that the partial volume change from $\overline{V}_{Sn}^4$ to $\overline{V}_{Sn}^3$ takes place before the Sn transport through the I_3-interface.

- The second step of the procedure is related to the stress relaxation induced by the depletion and the excess of the Sn atoms within the $Sn_{(l)}$ phase and the Cu_3Sn-phase, respectively. The tensile stress, induced by the depletion of the Sn atoms within the $Sn_{(l)}$ phase (i=4), can relax through the I_4-interface displacement $\Delta X_{I_4}^{R/L}$ during time increment Δt. It is defined as follows.

$$\Delta X_{I_4}^{R/L}(t) = J_{Sn/L}^4(X_{I_3},t)\times\overline{V}_{Sn}^4\times\Delta t \qquad (15)$$

The compressive stress, induces by the excess of Sn atoms within the Cu_3Sn-phase (i=2), can potentially relax through both Cu_6Sn_5 phase and $Cu_{(s)}$-phase. Nevertheless, in the case where the Cu_6Sn_5-phase is bridging the two IMCs layers, the relaxation through the $Cu_{(s)}$ phase can be favored expecting negligible strain because of the large dimension of this $Cu_{(s)}$ phase compared to that of the Cu_6Sn_5-phase. This relaxation thus involved a displacement $\Delta X_{I_1}^{R/L}$ of the I_1-interface during time increment Δt defined as:

$$\Delta X_{I_1}^{R/L}(t) = J_{Sn/L}^2(X_{I_1},t)\times\overline{V}_{Sn}^2\times\Delta t\,. \qquad (16)$$

The open boundary condition, at the cut-off I_0-interface, makes that an output of $Cu_{(s)}$-phase amount at constant $x_{Sn}^1(I_0)$-fraction equivalent to the length $\Delta X_{I_0}^{R/L} = \Delta X_{I_1}^{R/L}$ allows obtaining a zero strain within this $Cu_{(s)}$-phase.

- The third step of the procedure is related to the displacements of the interfaces I_3 and I_2 induced by the phase transformations within the $Sn_{(l)}$ and Cu_3Sn phases. The $\Delta X_{I_3}^{L}(t)$-displacement, induced by the

precipitation of the $Cu_6Sn_{4.99}$ compound (stoichiometry defined in relation with the molar fraction $x_{Sn}^{3}(I_3)$) at the I_3-interface from the Sn under saturated solution, is determined through the relation:

$$\Delta X_{I_3}^{L}(t) = X_{I_4}(t) + \Delta X_{I_4}^{R/L}(t) - X_{I_3}(t) - \frac{\left(6N_{Sn}^{4}(t) - 4.99N_{Cu}^{4}(t)\right)\times V_a^4(I_3)}{6C_{Sn}^{4}(I_3) - 4.99C_{Cu}^{4}(I_3)}, \quad (17)$$

where $N_{Sn}^{4}(t)$ and $N_{Cu}^{4}(t)$ are the initial Sn and Cu molar quantities per unit area defined as follows.

$$N_{Sn}^{4}(t) = C_{Sn}^{4}(I_3)\times\left(X_{I_4}(t) - X_{I_3}(t)\right) + J_{Sn/L}^{4}(X_{I_3}, t)\times\Delta t \quad (18)$$

$$N_{Cu}^{4}(t) = C_{Sn}^{4}(I_3)\times\left(X_{I_4}(t) - X_{I_3}(t)\right) \quad (19)$$

Similarly, we calculate the $\Delta X_{I_2}^{L}(t)$-displacement of the I_2-interface relative to the growth of the $Cu_6Sn_{4.81}$ compound (stoichiometry defined in relation with the molar fraction $x_{Sn}^{3}(I_2)$) at the I_2-interface from the Sn over-saturated solution through the relation,

$$\Delta X_{I_2}^{L}(t) = X_{I_2}(t) - (X_{I_1}(t) + \Delta X_{I_1}^{R/L}(t)) - \frac{\left(6N_{Sn}^{2}(t) - 4.81N_{Cu}^{2}(t)\right)\times V_a^2(I_2)}{6C_{Sn}^{3}(I_2) - 4.81C_{Cu}^{3}(I_2)}, \quad (20)$$

where the initial Sn and Cu molar quantities per unit area, $N_{Sn}^{2}(t)$ and $N_{Cu}^{2}(t)$ within the Cu_3Sn phase are defined as follows.

$$N_{Sn}^{2}(t) = \frac{C_{Sn}^{2}(I_2) + C_{Sn}^{2}(I_1)}{2}\left(X_{I_2}(t) - X_{I_1}(t)\right) - J_{Sn/L}^{2}(X_{I_2}, t)\times\Delta t \quad (21)$$

$$N_{Cu}^{2}(t) = \frac{C_{Cu}^{2}(I_2) + C_{Cu}^{2}(I_1)}{2}\left(X_{I_2}(t) - X_{I_1}(t)\right) \quad (22)$$

- The fourth step of the procedure is to calculate the additional displacements of the I_3 and I_4-interfaces induced by the change of partial molar volumes of Sn and Cu-atoms during precipitation (Eq. (4b)). These displacements are here written as:

$$\Delta X_{I_4}^{R_2/L} = \Delta X_{I_3}^{R_1/L} = -\left(\frac{x_{Sn}^{4}(I_3)}{V_a^4(I_3)}(\overline{V}_{Sn}^{4} - \overline{V}_{Sn}^{3}) - \frac{(1 - x_{Sn}^{4}(I_3))}{V_a^4(I_3)}(\overline{V}_{Cu}^{4} - \overline{V}_{Cu}^{3})\right)\Delta X_{I_3}^{L} \quad (23)$$

Finally, the position $X_{I_i}(t+\Delta t)$ of the I_i-interface (i=1,4) at time $t + \Delta t$ can be calculated from the position of the interface $X_{I_i}(t)$ at time t through the equation:

$$X_{I_i}(t+\Delta t) = X_{I_i}(t) + \Delta X_{I_i}^{R/L}(t) + \Delta X_{I_i}^{L}(t) + \Delta X_{I_i}^{R_1/L}(t) + \Delta X_{I_i}^{R_2/L}(t).$$

4. Simulation results and discussion

As we have seen, the IMC growth is the result of numerous reactions, kinetic and thermodynamic processes which for most of them superimpose. In this part we will discuss, in the light of experimental results, the modeling results of IMC growth based on different assumptions of diffusion mechanisms in order to propose a realistic scenario for IMC and micro-void formation.

- It is shown the simulations of IMC growth until the Sn liquid phase is consumed for different assumptions of diffusion mechanisms through the Cu_6Sn_5 layer. Volume diffusion is supposed to be the predominant mechanism within the Cu_3Sn-phase. The initial layer thicknesses of each involved phases are the average ones that we have measured from our experiments just after the heating rate (250°C). They are the result of the fast precipitation of the Cu_6Sn_5-phase from the Cu-oversaturated $Sn_{(l)}$-solution. The phase growth evolutions were calculated from the concentration profile drawn in figure 4 and using the inter-diffusion coefficients and the partial volumes of Cu and Sn-atoms indicated in Table 2. In these calculations, we take account of the elastic strain relaxation induced by the difference between the Cu and Sn partial molar volumes from the liquid phase to the IMC phases for one part, and from the $Cu_{(s)}$ phase to the IMC phases on the other part. The shrinkage relative to this relaxation at the Cu_3Sn-$Cu_{(s)}$ interface and through the $Cu_{(s)}$-phase is counterbalanced by the contact pressure used. No pore space can thus develop at the $Cu_{(s)}$-boundary. The shrinkage $\Delta X_{I_4}^{R_2}(t) = \Delta X_{I_3}^{R_1}(t)$, relative to the relaxation at the Cu_6Sn_5-$Sn_{(l)}$ interface through the $Sn_{(l)}$ phase (see paragraph 3.2.3) is shown in Fig. 7a and Fig. 7b between the dashed line (system symmetry) and the $Sn_{(l)}$-phase. The total displacement $\Delta X_{I_4}^{R2}(t) + \Delta X_{I_4}^{R/L}(t)$ involving the additional displacement $\Delta X_{I_4}^{R/L}$ of the I_4-interface, due to the depletion of the Sn atoms within the $Sn_{(l)}$ phase (i=4), (which could be also considered as vacancy aggregation), is shown in Fig. 7c.

Before the impingement of the two opposite layers, the development of the pore space is counterbalanced by the contact pressure. After the Cu_6Sn_5-scallop impingement, which constrains the reaction to take place into a fixed volume, the shrinkage leads to void formation until the consumption of the $Sn_{(l)}$ phase. This void is drawn in red in figure 7. We expect, in the light of experiments, that impingement occurs for similar thicknesses (6 μm) of Cu_6Sn_5 and $Sn_{(l)}$ layers.

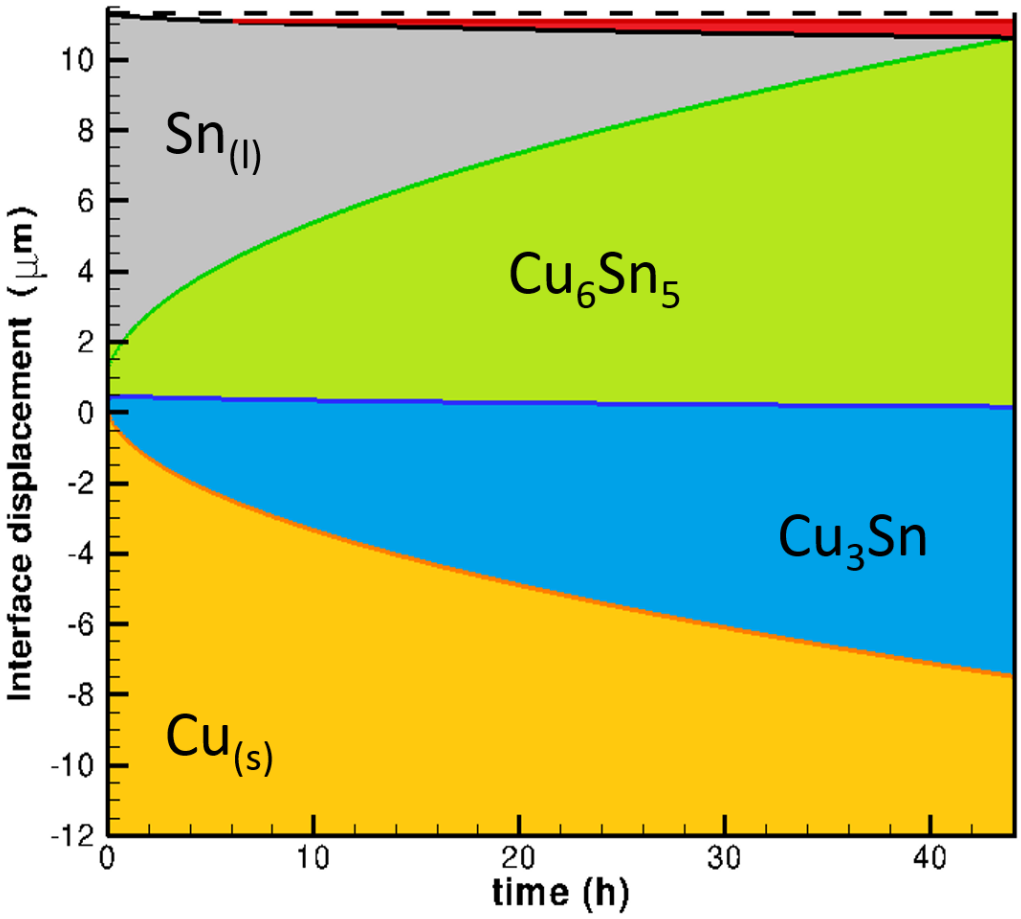

a)

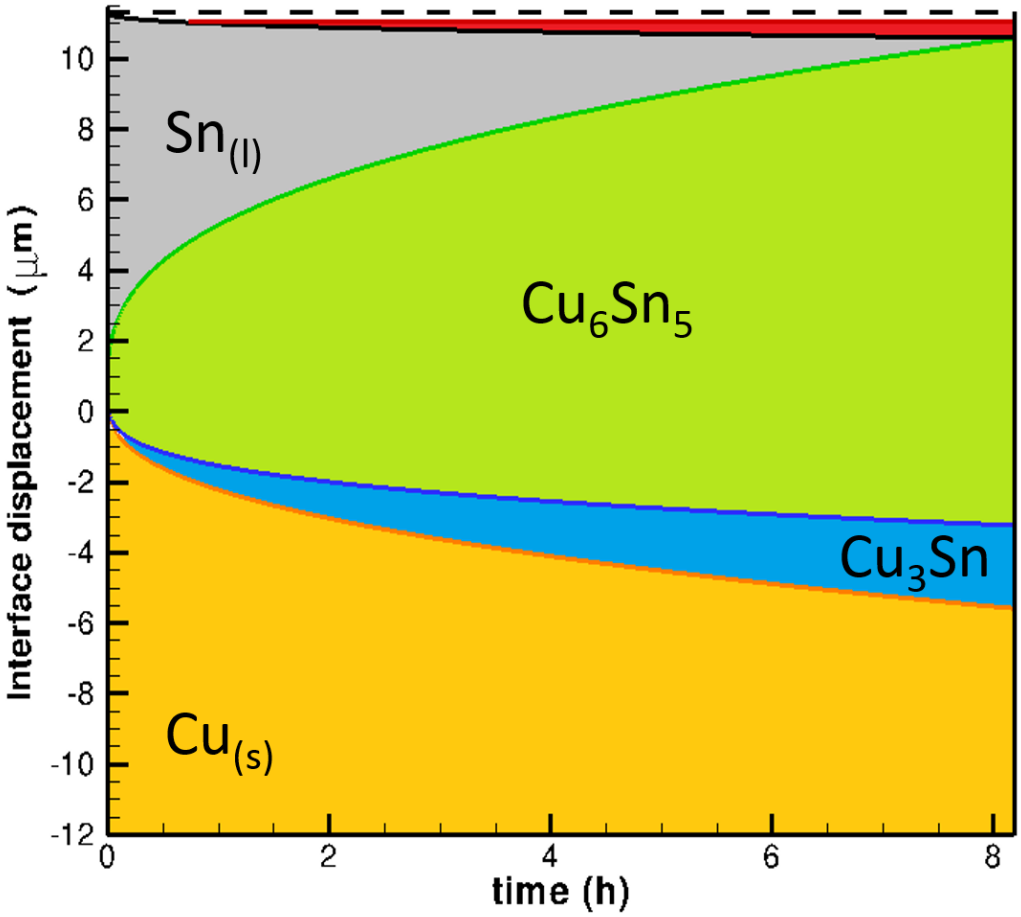
Sn(l)
Cu6Sn5
Cu3Sn
Cu(s)
Interface displacement (μm)
time (h)
10
8
6
4
2
0
-2
-4
-6
-8
-10
-12
0
2
4
6
8

457

458 b)

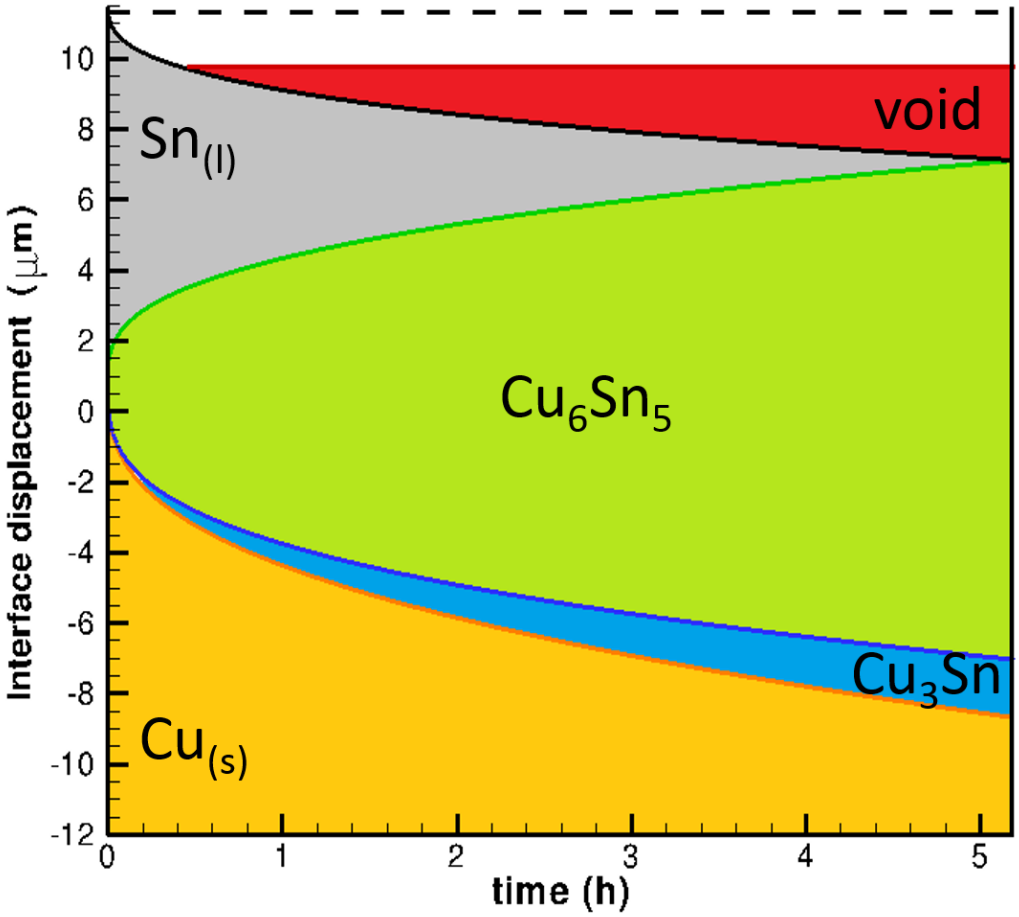
void
Sn(l)
Cu6Sn5
Cu3Sn
Cu(s)
Interface displacement (μm)
time (h)
10
8
6
4
2
0
-2
-4
-6
-8
-10
-12
0
1
2
3
4
5

459

460 c)

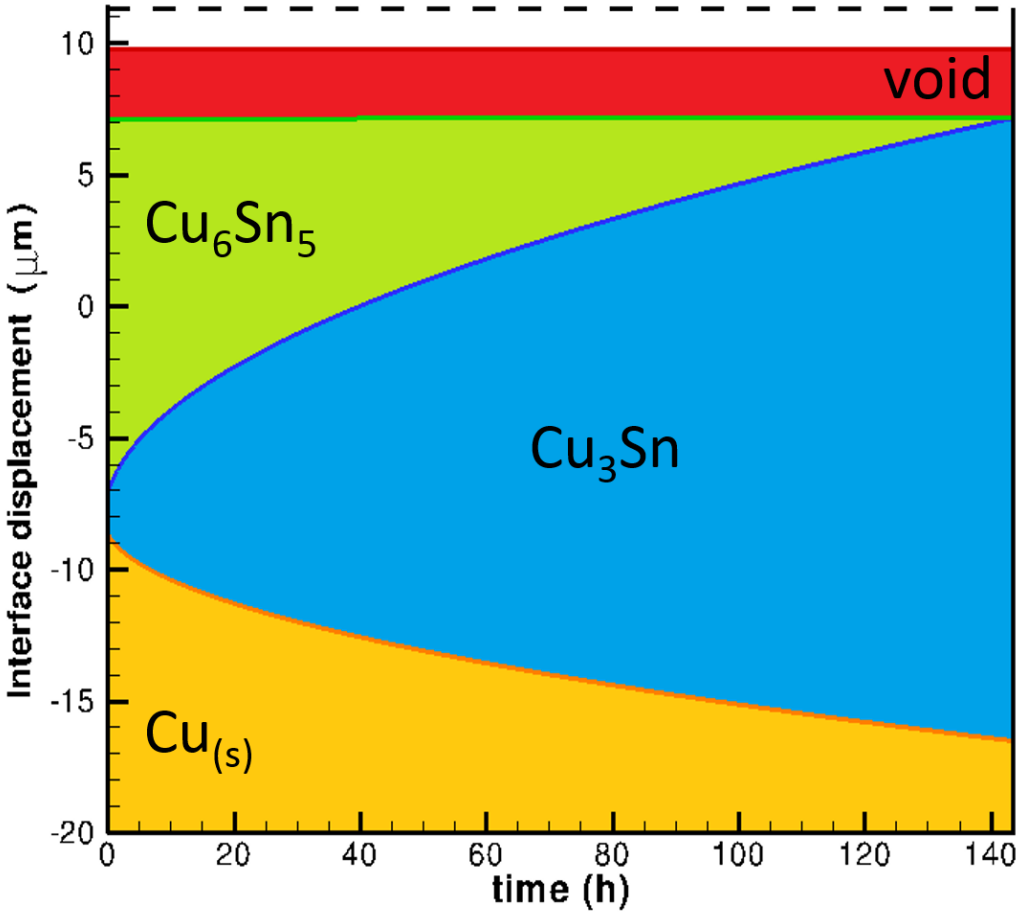

d)

Figure 7: Evolution of the interface displacements and void formation involved in the Cu/Sn-based solder joint for different mass transport scenarios taking account for volume shrinkage induced by the difference of Cu and Sn-partial molar volumes between each phase. Inter-diffusion of Cu and Sn-atoms is considered except for the simulation case (d). The bulk Cu and Sn-inter-diffusion coefficients as well as the partial molar volumes of Cu and Sn-atoms relative to each involved phase are indicated in table 2.

4.1- Interface evolution controlled by volume diffusion through the Cu_6Sn_5-layer

We show in figure 7a the modelling of the IMC growth in the Sn-based solder/Cu system until the $Sn_{(l)}$-phase is consumed.

First of all, we compare our results of phase change evolution with that reported in reference [33] in which similar constants to ours was considered: same atomic molar volume V_a^i for each *i*-phase; close ratio of inter-diffusion coefficient of Cu_6Sn_5 phase to that of Cu_3Sn one ($D^3/D^2 = 2.4$ for the present work and $D^3/D^2 = 2.1$ in reference [33]). In the modeling study of reference [33], the authors solved the same one-dimensional diffusion problem, with real molar volumes for the different phases, and quantified the pore volume formation. They used a fixed grid discretization allows to deal with more realistic molar fraction profiles than those here considered. Nevertheless, the present simplified profiles give rise to consistent results with regards to: i) the evolving ratio of the thickness of the Cu_3Sn-layer to that of Cu_6Sn_5, ii) the nearly constant position of the Cu_3Sn/Cu_6Sn_5 interface during phase change and iii) the non-dimensional time $t \times D^3/e^2 \approx 11$ for the Cu_6Sn_5 phase to reach the thickness e = 10 μm.

The comparison of the simulated results with experiment ones, for IMC growths, shows that the elapse time for the $Sn_{(l)}$-phase to be consumed is largely overestimated in the modeling (about twenty times greater), and that the experimental inhibition of the Cu_3Sn phase growth is not matched. This suggests that the Cu and Sn fluxes arriving at the Cu_3Sn-Cu_6Sn_5 interface from the Cu_6Sn_5-phase i.e. $J_{Sn}^3(X_{I_2}, t)$, should be greater to inhibit the Cu_3Sn-phase growth and to accelerate the overall phase change kinetics. Therefore, the dominant kinetic mechanism is supposed to be different from simple volume diffusion in the Cu_6Sn_5 phase in agreement with many experimental and modeling results [2, 18].

The void formation after the impingement of the two opposite layers corresponds to about 2.5 % of the total IMC and void layer (red zone in Figure 7a).

4.2- Interface evolution with competitive grain boundary diffusion limited by coarsening through the Cu_6Sn_5 phase

The competition between volume diffusion and grain boundary, limited by grain coarsening, is modeled using Eq. (8). The Cu_6Sn_5 grain size *d* (Fig. 5) will here be greater than 1 μm, during the overall growth, implying negligible grain boundary fraction $f \approx 0$ Eq. (6). The value we take for the grain boundary

498 factor $\frac{\delta R_D}{\sqrt{3}R} = 5.8\times10^{-5}$ in Eq. (8) is realistic since it corresponds to grain boundary width $\delta = 1\,\mathrm{nm}$

499 [36], grain boundary to volume diffusion coefficient ratio $R_D = \frac{D_{GB}^3}{D^3} = 10^4$ [37], and grain boundary

500 length to layer thickness ratio $R = \frac{d_{GB}}{d_L} = 0.1$. These values agree with experimental analysis. The

501 grain boundary diffusion mechanism predominates when $\frac{\delta R_D}{\sqrt{3}\,\mathrm{R}\left(X_{I_3}(t) - X_{I_2}(t)\right)} > 1$ (see Eq. (8)),

502 leading to a Cu_6Sn_5 layer thickness $d_L = \left(X_{I_3}(t) - X_{I_2}(t)\right)$ lower than 58 μm. Since it is the case for the

503 present system dimensions, grain boundary mechanism is the one which predominates during the

504 diffusion process through the Cu_6Sn_5 layer. This condition is consistent with kinetics studies that have

505 shown that Cu_6Sn_5 growth is dominated by grain boundary diffusion limited by coarsening [2, 18].

506

507 The IMC growth modeled with such predominant grain boundary diffusion mechanism is shown in

508 figure 7b. The main point that we can notice is that the grain boundary mechanism allows to model the

509 inhibition of the Cu_3Sn-growth through larger $J_{Sn}^3(X_{I_2}, t)$-flux at the Cu_6Sn_5-Cu_3Sn interface compared

510 to that involved for volume diffusion only as previously shown in figure 7a. The inhibition of the Cu_3Sn

511 growth reduces with time as the grain boundary flux decreases consequently to the grain coarsening

512 process. In fact, the ratio of the grain boundary flux to volume flux is 58 (d=1 μm) for the initial time

513 and decreases to about 4.5 (d = 13 μm) for the end time.

514 If grain boundary diffusion allows to well model the inhibition of Cu_6Sn_5-growth with process time of

515 the order of magnitude of experimental one, this mechanism nevertheless still fails in representing the

516 large pore space obtained when the $Sn_{(l)}$ phase is entirely consumed. The fraction of void is like that

517 obtained when the volume diffusion is the only mechanism involved (see for comparison figure 7a).

518 Similarly to the previous modelling case based on volume diffusion mechanism, only (see for

519 comparison figure 7a) the pore volume which develops after the Cu_6Sn_5 bridge formation (visualized in

520 red) reaches about 2.5% of the total IMCs and void layer at the end of the process. This pore volume is

the result of volume shrinkage induced by the difference in partial molar volume of atoms between the reacting phases and the IMCs that we account for in this model. More precisely, the pore formation is induced by the partial molar volume change of Sn at the $Cu_6Sn_5/Sn_{(l)}$ interface. The effect of partial molar volume change of Cu atoms at the Cu_3Sn/Cu interface does not contribute to the pore formation since the Cu substrates are free in the perpendicular direction.

4.3- Additional mechanism involving inter-diffusion of Sn/vacancies couple within the Cu_6Sn_5 phase.

The use of inter-diffusion coefficient is just like to any Sn fluxes, is associated with reverse Cu-fluxes of equal intensity. The intrinsic diffusion coefficient of Cu and Sn-atoms relative to the Cu_6Sn_5-phase, respectively D_{Cu}^3 and D_{Sn}^3, are thus hidden through this apparent inter-diffusion coefficient written as, D^3. In presence of vacancies and when one component diffuses faster than the others, Kirkendall voids can form behind the migration of the atoms which diffuse faster. Here, in the case of the Cu and Sn-based solder, voids are in the middle of the Cu_6Sn_5-interlayer sustaining our hypothesis of Sn-atoms as the faster diffusing components, as was shown in some studies [18, 32]. The inter-diffusion of Sn atoms with vacancies is modeled through equations described in paragraph 3.2.4. Same predominant grain boundary diffusion limited by grain growth was considered using Eq. (8) and similar values for the δ, R_D, R-constants as previously defined in paragraph 4.2. We also assumed that Sn/vacancy inter-diffusion coefficient $D_{Sn/L}^3$ is twice greater than the Sn/Cu inter-diffusion coefficient D^3 ($D_{Sn/L}^3 = 2D^3$). In this condition, 1/3 of the diffusion within the Cu_6Sn_5-phase is devoted to the Sn and Cu inter-diffusion and 2/3 to the Sn/vacancy one.

IMC growth modeled with such additional Sn/vacancy inter-diffusion with predominant grain boundary diffusion through the Cu_6Sn_5 phase, is shown in figure 7c. First, we can notice that the formation of the void space from the impingement time is largely amplified. This void space, drawn in red, reaches 14 % of the total IMC and void layer which is close to experimental data. Note that the volume shrinkage

participates to only 18% of the void volume formation. The remaining 82% of the void is the result of the IMC preferential growth towards the $Cu_{(s)}$-phase which is correlated to the aggregation of vacancies interlayer. Secondly, we can notice that the inhibition of the Cu_3Sn growth, when grain boundary diffusion is active (paragraph 4.3.2), remains and is even enhanced with Sn/vacancy inter-diffusion. The total IMC/void thickness, close to 20 μm, is consistent with the experimental dimension of this layer.

Therefore, we can confirm that the large void formation can be explained by greater $Sn_{(l)}$ fluxes than $Cu_{(l)}$ fluxes through the Cu_6Sn_5 phase which are mainly located along the grain boundaries. This agrees with the conclusions of other papers [25, 32] which state that the accumulation of Sn atoms at the Cu_6Sn_5 boundary is the driving force for IMC growth. In these conditions, the reaction, 2 Cu_3Sn + 3 Sn → Cu_6Sn_5, at the Cu_6Sn_5-Cu_3Sn interface, is favored instead of the Cu_6Sn_5 precipitation at the Cu_6Sn_5-$Sn_{(l)}$ interface.

This is also in agreement with large void formation in the Cu_6Sn_5-phase induced by electro-migration which enhances the diffusion of Sn atoms compared to that of Cu atoms at a temperature below the melting point [38].

4.4. Final step up to the equilibrium state

Further interface evolution, at 250°C, when the $Sn_{(l)}$-phase is consumed, is shown in Fig. 7d. The initial phase-thicknesses are that obtained at the end time of figure 7c for the case where Sn/vacancy inter-diffusion is considered. The calculation was done from the concentration profile within the Cu_3Sn-phase drawn in figure 4 except for the Cu_6Sn_5 layer where the Sn molar concentration is now taken constant $C^4_{Sn}(X,t) = C^4_{Sn}(I_3)$ since it is bounded by Cu_3Sn-Cu_6Sn_5 interfaces only. No mass transport within the Cu_6Sn_5-phase is thus involved during this last step. No shrinkage relative to the liquid/solid phase change has to be considered.

The modeling results clearly show the growth of the Cu_3Sn layer at the expense of Cu_6Sn_5 layer in agreement with experimental results, the pore volume remaining constant. It finally represents around 10 % of the Cu_3Sn-layer thickness. Simulation kinetics show that the time to reach the final stable state, where the Cu_6Sn_5 IMC is entirely consumed, is very long at 250°C (about 140 h). Same order of

574 magnitude was predicted for the phase-field simulations of Park et al [10] for T=260°C and similar
575 initial Sn layer thickness (25 μm). These results suggested that the dominant kinetic mechanism in the
576 Cu_3Sn phase is bulk diffusion [2, 5, 11, 20, 26].
577

578 **5. Conclusion**

579 The growth and the morphology of the Cu_3Sn and Cu_6Sn_5 phases, during the TPL bounding of Cu-Sn-
580 Cu sandwich structures, was investigated through both experimental and modeling approaches. The
581 experiments were carried out with process parameters favoring void formation (temperatures of 250 °C,
582 270 °C, 300 °C, pressure loading of 5 kPa, Sn foil thickness of 10 μm) allowing to clearly exhibit the
583 key role of the scallop-type morphology of the Cu_6Sn_5 intermetallic. This morphology favored early
584 impingement and constrained, from that time, the Cu_6Sn_5 growth evolve into a fixed and large volume
585 of $Sn_{(l)}$ phase. The pore formation is shown to start from that impingement time near the Cu_3Sn IMC in
586 between 2 Cu_6Sn_5 scallops and to grow until the $Sn_{(l)}$ phase is totally consumed. The volume fraction of
587 pores, inside the IMC layer, is ranging from 10 % to 20%. The growth of the Cu_3Sn phase is shown to
588 be inhibited until the complete consumption of the $Sn_{(l)}$ phase and to evolve from that time with a planar
589 surface.
590 The modeling of the IMC growth was based on i) the diffusion mass transport as limiting process, ii)
591 the rate of interface displacement depending on the local equilibrium at the interface and finally iii) the
592 shrinkage induced by the difference of partial molar volumes of atoms between the $Cu_{(s)}$ and $Sn_{(l)}$ phases
593 and the IMCs. The simulations were reduced to a 1D-problem corresponding to the experimental
594 sequence of phase layers and including the potential development of a void space. The evolution of the
595 IMC growth was simulated, assuming saturations of the $Cu_{(s)}$ and $Sn_{(l)}$ solutions, from the experimental
596 IMC thicknesses (average layer thickness for Cu_6Sn_5) analyzed for 250°C temperature and 0 min holding
597 time up to the final equilibrium state corresponding to a complete transformation of Cu_6Sn_5 to Cu_3Sn.
598 Several mass transport scenarios have been simulated depending on i) the type of inter-diffusions,
599 (exchange between Cu and Sn atoms and/or exchange between Sn atoms and vacancies) and ii) the type
600 of diffusion mechanisms (volume diffusion for both IMC layers or volume diffusion for Cu_3Sn layer

601 and boundary diffusion limited by grain growth for Cu_6Sn_5 layer). Within this 1D solving procedure,
602 the latter diffusion mechanism was modeled through the introduction of an analytic function in the flux
603 equation. This function tries to describe the scallop morphology of the Cu_6Sn_5 layer, with time through
604 the ratio of the grain boundary length to the grain size (R = 0.1), assuming equiaxed grains. Realistic
605 values of the other function parameters were taken, δ = 1 nm for the grain boundary width and $R_D = 10^5$
606 for the ratio of grain boundary diffusion coefficient to volume diffusion coefficient.
607 The comparisons of simulation and experimental results have shown that:
608 i) The inter-diffusion of Cu and Sn atoms, along the shortened grain boundaries of Cu_6Sn_5 layer,
609 enhanced the displacement rate of the Cu_3Sn-Cu_6Sn_5 interface in the direction of Cu_3Sn phase compared
610 to volume diffusion. This behavior induced the observed growth inhibition of that latter IMC.
611 ii) The formation of micro-pores, inside the interlayer, is mainly driven by the inter-diffusion of
612 Sn atoms with vacancies along the Cu_6Sn_5 grain boundaries and not to the volume shrinkage induced by
613 the difference of partial molar volumes of atoms between each phase. When 2/3 of the diffusion is
614 devoted to the Sn and vacancies inter-diffusion and 1/3 to the Sn and Cu one, void space, inside the IMC
615 layer, reach 14% of volume fraction. This value closely matches the experimental analyzed values. This
616 mechanism of Kirkendall pore formation requires that Sn atoms diffuse faster that Cu ones through
617 Cu_6Sn_5 layer, which tends to favor the growth of Cu_6Sn_5 IMC towards the $Cu_{(s)}$ phase rather the $Sn_{(l)}$
618 one.
619

620 **5. References**

621 [1] P. Beckedahl, Power Electron. Europe, 2011, **5**, 23 (http://www.power-
622 mag.com/pdf/issuearchive/47.pdf)
623 [2] J.F. Li, P.A. Agyakwa, C.M. Johnson, Acta Mater., 2011, **59**, 1198
624 [3] T.B. Massalski, Binary alloy phase diagrams. (ASM Int. Materials Park, Ohio, 1990), pp. 1481-
625 1483
626 [4] S. Fürtauer, D. Li , D. Cupid, H. Flandorfer, Intermetallics, 2013, **34**, 142
627 [5] C. Flötgen, M. Pawlak, E. Pabo, Microsyst. Technol., 2014, **20**, 653
628 [6] W.-L. Chui, C.-M. Liu, Y.-S. Haung, C. Chen, Appl. Phys. Lett., 2014, **104**, 171902
629 [7] D. Ma, W.D. Wang, S.K. Lahiri, J. Appl. Phys., 2002, **91**, 3312
630 [8] N.S. Bosco, F.W. Zok, Acta Mater., 2004, **52**, 2965
631 [9] M.S. Park, R. Arróyave, Acta Mater., 2012, **60**, 923
632 [10] M.S. Park, S.L. Gibbons, R. Arróyave, Acta Mater., 2012, **60**, 6278
633 [11] M.S. Park, S.L. Gibbons, R. Arróyave, Microelectron. Reliab., 2014, **54**, 1401
634 [12] H. Shao, A. Wu, Y. Bao, Y. Zhao, G. Zou, Mater. Sc. Eng. A, 2017, **680**, 221
635 [13] H.Y. Chuang, T.L. Yang, M.S. Kuo, Y.J. Chen, J.J. Yu, C.C. Li, C.R. Kao, IEEE Trans. Device
636 Mater. Reliab., 2012, **12**, 233
637 [14] Z. Mei, A.J. Sunwoo, J.W. Morris, Metall. Trans. A, 1992, **23**, 857
638 [15] E. Kirkendall, Trans. AIME, 1947, **147**, 104
639 [16] F. Gao, J. Qu, Mater. Lett., 2012, **73**, 92
640 [17] M. O, G. Vakanas, N. Moelans, M. Kajihara, W. Zhang, Microelectron. Eng., 2014, **120**, 133
641 [18] A. Paul, C. Ghosh, W.J. Boettinger, Metall. Mater. Trans. A, 2011, **42A**, 952
642 [19] K.N. Tu, R.D. Thompson, Acta Metall.,1982, **30**, 947
643 [20] S. Kumar, C.A. Handwerker, M.A. Dayananda, J. Phase Equilib. Diff., 2011, **32**, 309
644 [21] D.S. Duvall, W.A. Owczarsk, D.F. Paulonis, Weld. J., 1974, **53**, 203
645 [22] L. Bernstein, J. Electrochem. Soc., 1966, **113**, 1282
646 [23] I. Tuah-Poku, M. Dollar, T.B. Massalski, Metall. Trans. A, 1988, **19A**, 675
647 [24] G.O. Cook, C.D. Sorensen, J. Mater. Sc., 2011, **46**, 5305

[25] M. Schaefer, R.A. Fournelle, J. Liang, J. Electron. Mater., 1998, **27**, 1167

[26] B. Dimcic, R. Labie, J. De Messemaeker, K. Vanstreels, K. Croes, B. Verlinden, I. De Wolf, Microelectron. Reliab., 2012, **52**, 1971

[27] K.L. Erickson, P.L. Hopkins, P.T. Vianco, J. Electron. Mater., 1994, **23**, 729

[28] P. Villars, L.D. Calvert, Pearson's handbook of Crystallographic Data for intermetallic Phases (ASM, Metals Park, Ohio, 1985), pp. 2030

[29] B. Alchagirov, A.M. Chochaeva, High Temp., 2000, **38,** 48

[30] M. Raessi, J. Mostaghimi, Numer. Heat Tr. Part B, 2005, **47**, 507

[31] J.A. Cahill, A.D. Kirshenbaum, J. Phys. Chem., 1962, **66**, 1080

[32] M. Onishi, H. Fujibuchi, Trans. JIM, 1975, **16**, 539

[33] J.F. Li, P.A. Agyakwa, C.M. Johnson, Intermetallics, 2013, **40**, 50

[34] K. Hoshino, Y. Iijima, K. Hirano, Trans JIM, 1980, **21**, 674

[35] C.A. Ma, R.A. Swalin, Acta Metall., 1960, **8**, 388

[36] D. Prokoshkina, V.A. Esin, G. Wilde, S.V. Divinski, Acta Mater., 2013, **61**, 5188

[37] Y. Zhou, T.H. North, Acta Metall. Mater., 1994, **42**, 1025

[38] R. An, Y. Tian, R. Zhang, J. Mater. Sci.: Mater. Electron., 2015, **26**, 2674

666 **Table**
667

668 Table 1: Sn-molar fractions at the different interfaces involved in the Cu-Sn system with reference to
669 the phase diagram for a temperature of 250 °C [3].

670

Interface	$Cu_{(s)}$-Cu_3Sn		Cu_3Sn-Cu_6Sn_5		Cu_6Sn_5-$Sn_{(l)}$	
Sn molar fraction	$x_{Sn}^{1}(I_1)$	$x_{Sn}^{2}(I_1)$	$x_{Sn}^{2}(I_2)$	$x_{Sn}^{3}(I_2)$	$x_{Sn}^{3}(I_3)$	$x_{Sn}^{4}(I_3)$
	2.2	23.6	24.7	44.5	45.4	97.8

671 Table 2: Partial molar volumes of Sn and Cu-atoms and inter-diffusion coefficients for the phases
672 involved in the Sn-based solder/Cu system: [a]deduced from the lattice parameter data available in the
673 literature [28]; [b]deduced from the density of liquid tin at 250°C [29] and from the 3% variation for the
674 liquid/solid transition as determined in [30] for the $Cu_{(s)}$-phase; [c]deduced from the density of copper at
675 250°C and from the extrapolation at 250°C of the linear variation of liquid copper density for the $Sn_{(l)}$-
676 phase [31]; [d]calculated at 250°C from Arrhenius equation defined in [14]. They are close to that we can
677 obtain from other references [32-33]; [e]calculated at 250°C from Arrhenius equation defined for 2% of
678 Sn in [34]; [f]close to $Sn_{(l)}$ self-diffusion coefficient [35].

Phase i	$Cu_{(s)}$ (i = 1)	Cu_3Sn (i = 2)	Cu_6Sn_5 (i = 3)	$Sn_{(l)}$ (i = 4)
Sn partial molar volume $\overline{V}_{Sn}^{i}$ (cm^3/mol)	16.3[b]	15.9[a]	15.9[a]	17.0[b]
Cu partial molar volume $\overline{V}_{Cu}^{i}$ (cm^3/mol)	7.1[c]	6.2[a]	6.2[a]	7,3[c]
Inter-diffusion coefficient D^i (m^2/s)	$1.0x10^{-22}$[e]	$3.6x10^{-15}$[d]	$7.6x10^{-15}$[d]	$2.0x10^{-9}$[f]

679

680

Figure captions

Figure 1: Different steps of the IMC report using TLPB based on Cu-Sn system. a) Fusion of the Sn filler metal (liquid Sn in blue color), b) Dissolution of part of the Cu substrate inside liquid Sn and nucleation of first Cu_6Sn_5 germs, c) Growth of both Cu_6Sn_5 and Cu_3Sn IMCs and consumption of remaining liquid Sn d) Complete consumption of liquid Sn and solidification of the IMC joint, e) Homogenization of the joint toward the most stable Cu_3Sn intermetallic, f) Cu-Sn binary phase diagram (Reprinted from reference [3]).

Figure 2: Experimental formation of Cu-Sn IMC joint for different holding time for a 5 KPa pressure and a holding temperature of 250°C. a) SEM micrograph at 0 min, b) AES line profile at 0 min, c) SEM micrograph at 15 min, d) SEM micrograph at 30 min, e) SEM micrograph at 45 min, f) SEM micrograph at after complete reaction of liquid Sn (2 hours)
Color scale (a-e) (darker to lighter gray): Cu substrate; Cu_3Sn; Cu_6Sn_5, Sn
Color scale (f) (darker to lighter gray): Cu substrate; Cu_3Sn; Cu_6Sn_5

Figure 3: Evolution of the IMC morphology and chemical composition with holding temperature (pressure of 5 KPa and holding time of 120 min): a) 250°C, b) 270°C and c) 300°C
Color scale (a-c) (darker to lighter gray): Cu substrate; Cu_3Sn; Cu_6Sn_5

Figure 4: One-dimensional problem of the Cu_6Sn_5 and Cu_3Sn layers in the Sn based solder-Cu system using linear profile of Sn molar concentrations $C_{Sn}^{i}(X,t)$ within each phase *i*.

Figure 5: Geometric model for the microstructure of the Cu_6Sn_5-layer described in [25]. (a), top view of the layer showing grain size *d* and grain boundary width δ. (b), cross section corresponding to the dashed line in (a) showing the average layer thickness d_L and the average grain boundary length d_{GB}.

→ Sn-fluxes in the bulk and along grain boundaries of the Cu_6Sn_5-layer and along the Cu_3Sn/Cu_6Sn_5 interface

→ Reverse Cu-fluxes of equal intensity in the case of inter-diffusion

Figure 6: Schematic illustration of the mechanism of Sn/vacancy inter-diffusion within the Cu_6Sn_5-phase involving Cu_6Sn_5-growth at the interfaces I_3 and I_2 together with displacements of the I_1 and I_4 interfaces. The I_4 interface displacement induces pore formation.

Figure 7: Evolution of the interface displacements and void formation involved in the Cu/Sn-based solder joint for different mass transport scenarios taking account for volume shrinkage induced by the difference of Cu and Sn-partial molar volumes between each phase. Inter-diffusion of Cu and Sn-atoms is considered except for the simulation case (d). The bulk Cu and Sn-inter-diffusion coefficients as well as the partial molar volumes of Cu and Sn-atoms relative to each involved phase are indicated in table 2.

(a), volume diffusion mechanism within both IMCs; (b) diffusion mechanism through the volume for Cu_3Sn and along the grain boundaries including grain growth for Cu_6Sn_5; (c), same diffusion mechanisms as in case (b) with 2/3 of the inter-diffusion devoted to the Sn/vacancy-exchange and 1/3 to the Sn and Cu one; (d) last step after the $Sn_{(l)}$-phase is consumed leading to the final stable state.